Electronic Supplementary Information (ESI)

Multistimuli-responsive multicolor solid-state luminescence tuned by NH-dependent switchable hydrogen bonds

Rui Zhang,[‡a] Li-Hua He,[‡a] Sui-Jun Liu,[a] Jin-Sheng Liao,[a] He-Rui Wen,[a] Jing-Lin Chen,*[a,b] and Feng Zhao*[c]

[a] *Jiangxi Provincial Key Laboratory of Functional Molecular Materials Chemistry, School of Chemistry and Chemical Engineering, Jiangxi University of Science and Technology, Ganzhou 341000, People's Republic of China*

[b] *State Key Laboratory of Structural Chemistry, Fujian Institute of Research on the Structure of Matter, Chinese Academy of Sciences, Fuzhou 350002, People's Republic of China*

[c] *School of Chemistry and Chemical Engineering, Jiangxi Science and Technology Normal University, Nanchang 330013, P.R. China*

EXPERIMENTAL SECTION

General Procedures and Materials. All reactions were performed under an N_2 atmosphere using solvents treated with an appropriate drying reagent. Commercially available reagents were used without further purification unless otherwise stated. 5-*Tert*-butyl-3-(2′-pyrimidinyl)-1*H*-1,2,4-triazole (bpmtzH) was synthesized according to the literature methods.[1]

Crystal Structural Determination. Crystal data were determined on a Bruker D8 QUEST diffractometer with a graphite-monochromated Mo Kα radiation (0.71073 Å). Structures were solved by direct method and refined by full-matrix least-squares technique on F^2 using the *SHELXTL* and *Olex*2 packages.[2-4] All non-hydrogen atoms were anisotropically refined, while hydrogen atoms were theoretically generated with isotropic thermal parameters.

Physical Measurements. ^{1}H NMR spectra were measured on Bruker Avance III NMR spectrometer. Infrared spectra were recorded on a Bruker Optics ALPHA FT-IR spectrometer using KBr pellets. Powder X-ray diffraction (PXRD) analyses were carried out on an Empyrean (PANalytical B.V.) diffractometer for a Cu-target tube and a graphite monochromator. Simulation of the PXRD patterns was performed by using single-crystal structure data and diffraction-crystal module of the Mercury (Hg) program version 3.0 available free of charge via the Internet at http://www.iucr.org. Thermogravimetric analysis (TGA) was performed on a PerkinElmer Pyris Diamond TG/DTA 6300 instrument under a nitrogen gas atmosphere at a heating rate of 10 ℃ min^{-1}. Solid-state luminescence properties were recorded on an Edinburgh F900 fluorescence spectrometer with a thermoelectrically cooled Hamamatsu R3809 photomultiplier tube. Solid-state emission quantum yield was measured by using an integrating sphere. The radiative decay rate constant k_r and non-radiative decay rate constant k_{nr} were calculated by $k_r = \Phi/\tau$ and $k_{nr} = (1-\Phi)/\tau$, respectively.[5,6]

Computational Methodology. The excited triplet state (T_1) geometries of **1c**, **1d**, and *ground* **1d** were optimized by using the B3LYP functional[7,8] with 6-31G(d) basis set[9] for H, C, N, F, and P and LANL2DZ basis set[10] for Cu. The lowest-lying vertical excitation energies ($S_0 \rightarrow T_1$) were calculated by time-dependent density functional theory (TDDFT) calculations[11,12] of the closed-shell state at the optimized T_1 state geometries using the M06-2X functional[13] with the same basis sets. All calculations were performed by using the Gaussian 16[14] in the gas phase. The electronic density plots for the frontier molecular orbitals were obtained by using Multiwfn 3.8 analyzer soft[15] and VMD program[16].

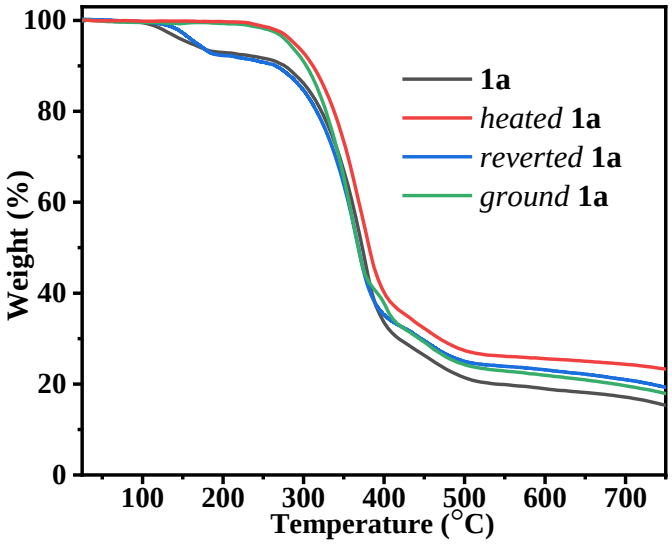

Fig. S1 TGA curves of **1a** in different solid states.

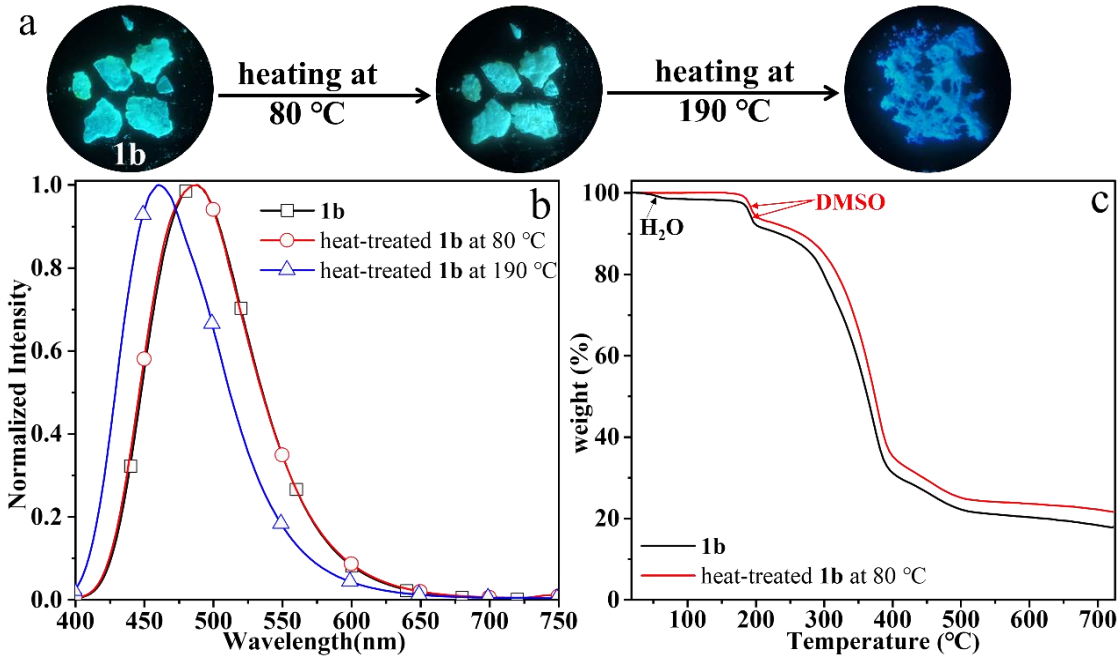

Fig. S2 Photographic images (a), emission spectra (b), and TGA curves (c) of **1b** in different solid states.

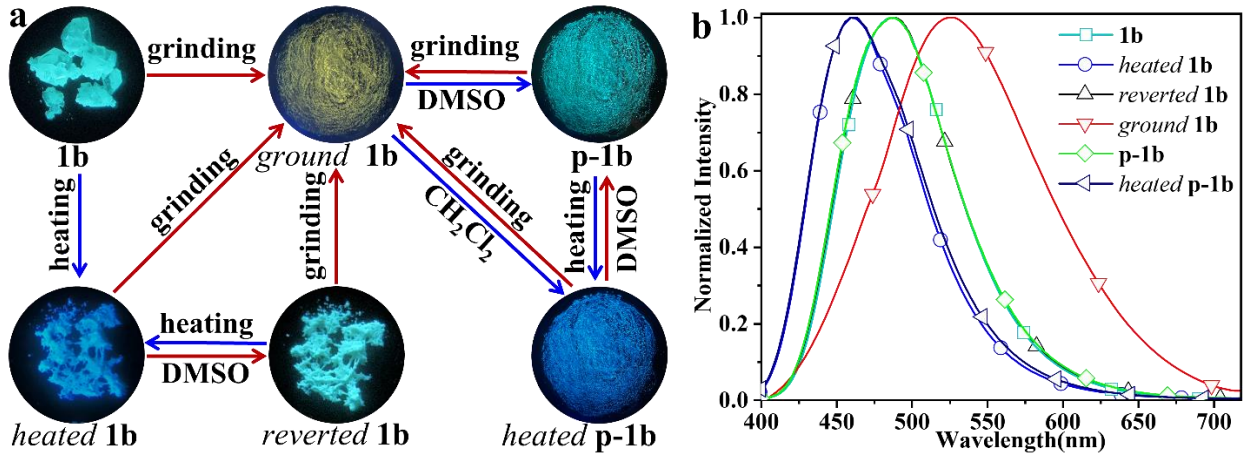

Fig. S3 Photographic images (a) and emission spectra (b) of **1b** in different solid states.

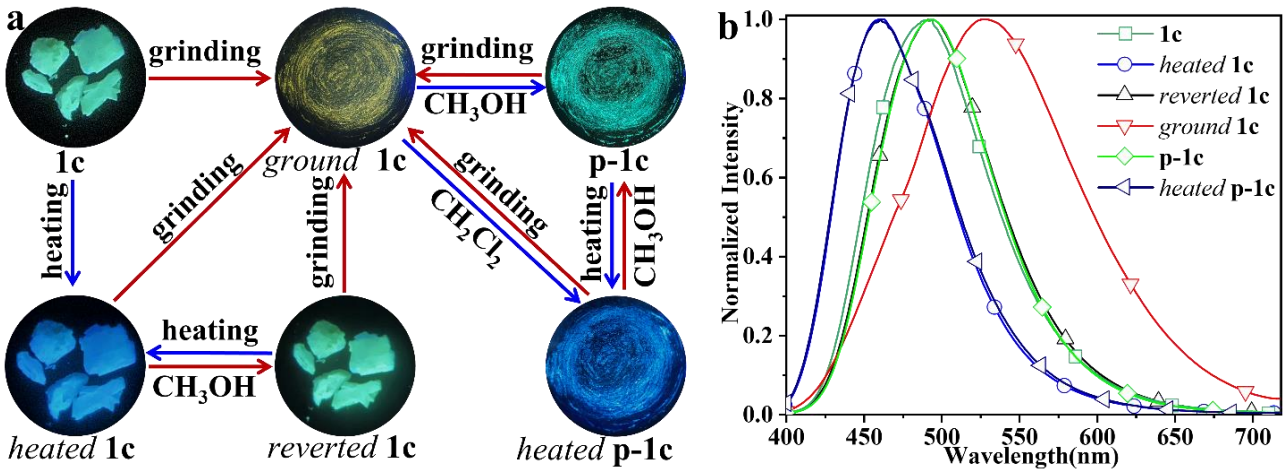

Fig. S4 Photographic images (a) and emission spectra (b) of **1c** in different solid states.

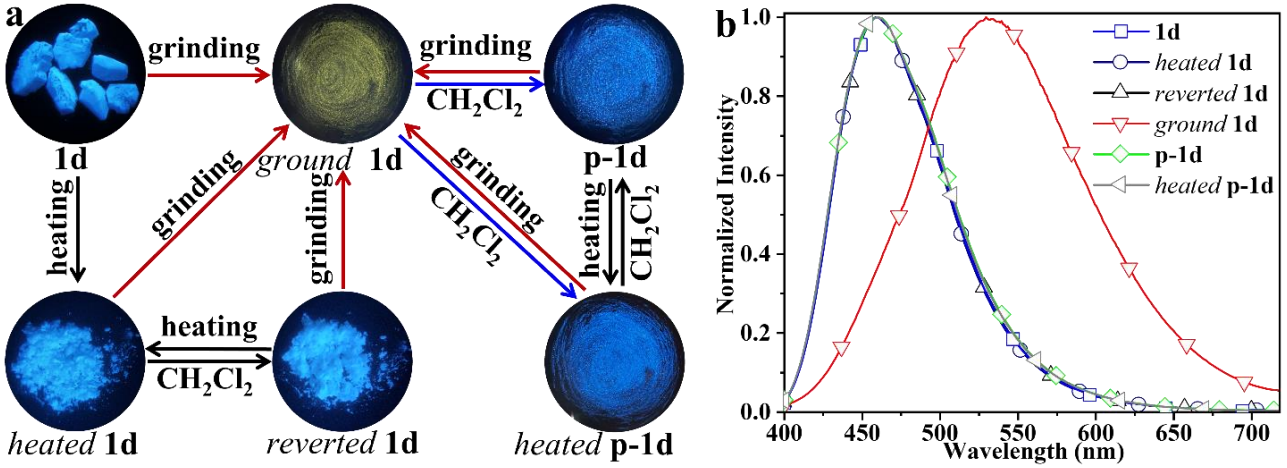

Fig. S5 Photographic images (a) and emission spectra (b) of **1d** in different solid states.

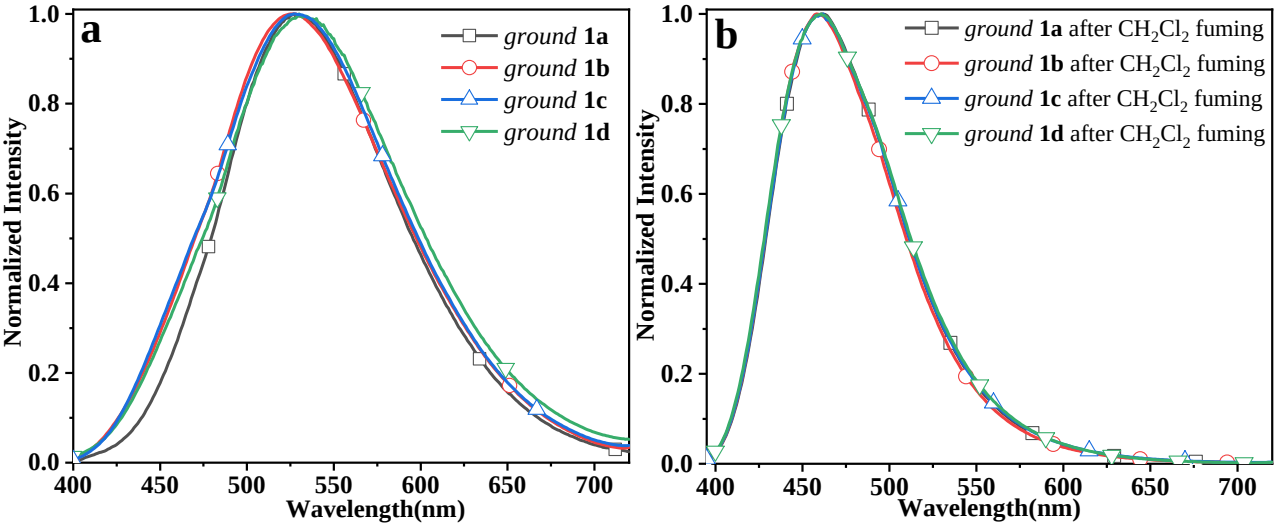

Fig. S6 Emission spectra of ground **1a–1d** (a) and *ground* **1a–1d** after CH_2Cl_2 fuming (b).

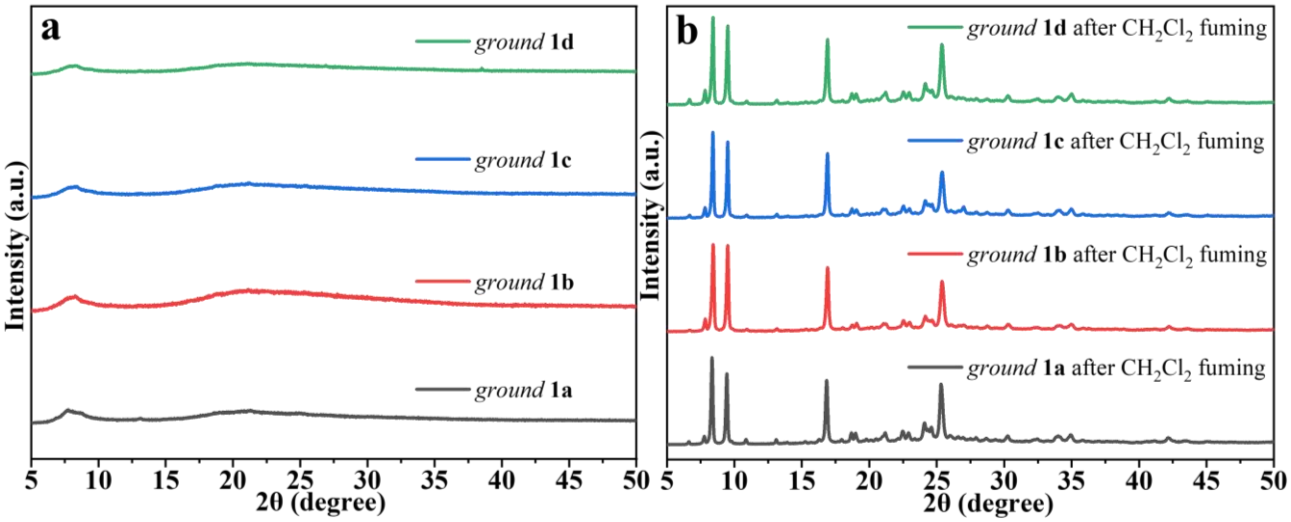

Fig. S7 PXRD patterns of *ground* **1a**–**1d** before (a) and after (b) CH_2Cl_2 fuming.

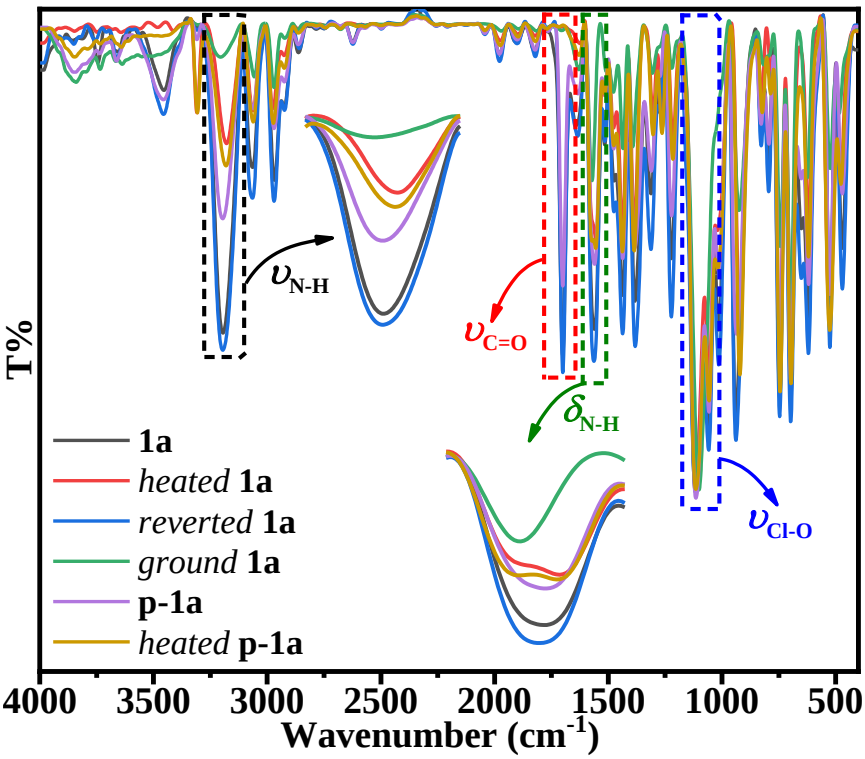

Fig. S8 FT-IR spectra of **1a** in different solid states.

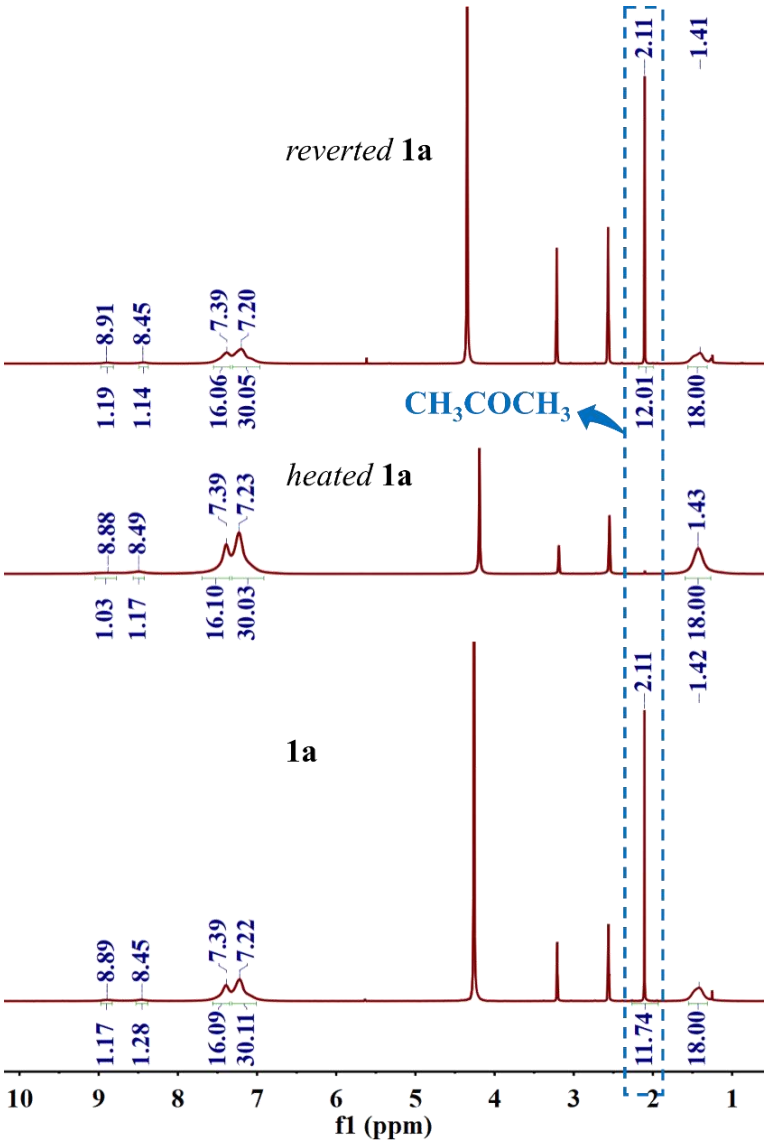

Fig. S9 ^{1}H NMR spectra of **1a**, *heated* **1a**, and *reverted* **1a** in CD_3OD/DMSO-d_6 (1:1 v/v).

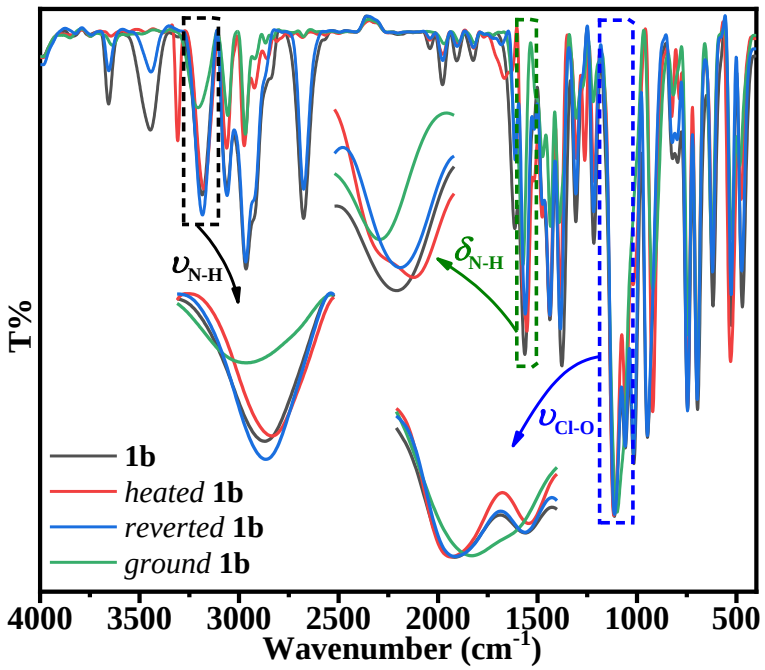

Fig. S10 FT-IR spectra of **1b** in different solid states.

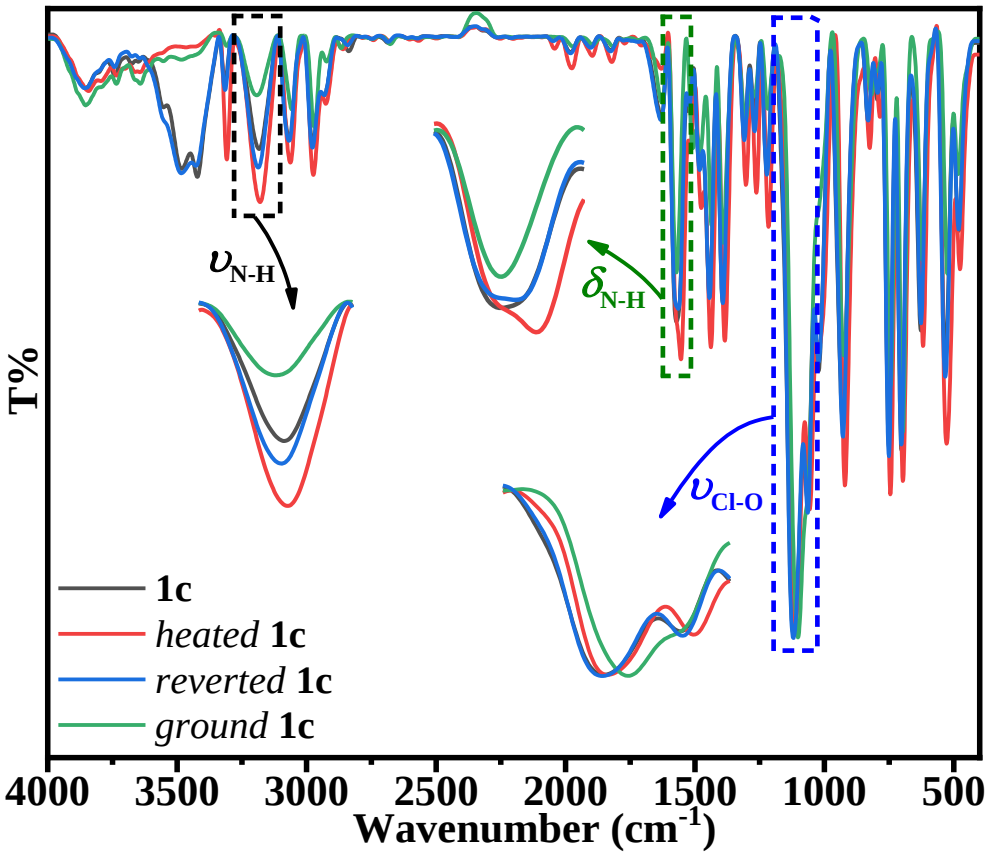

Fig. S11 FT-IR spectra of **1c** in different solid states.

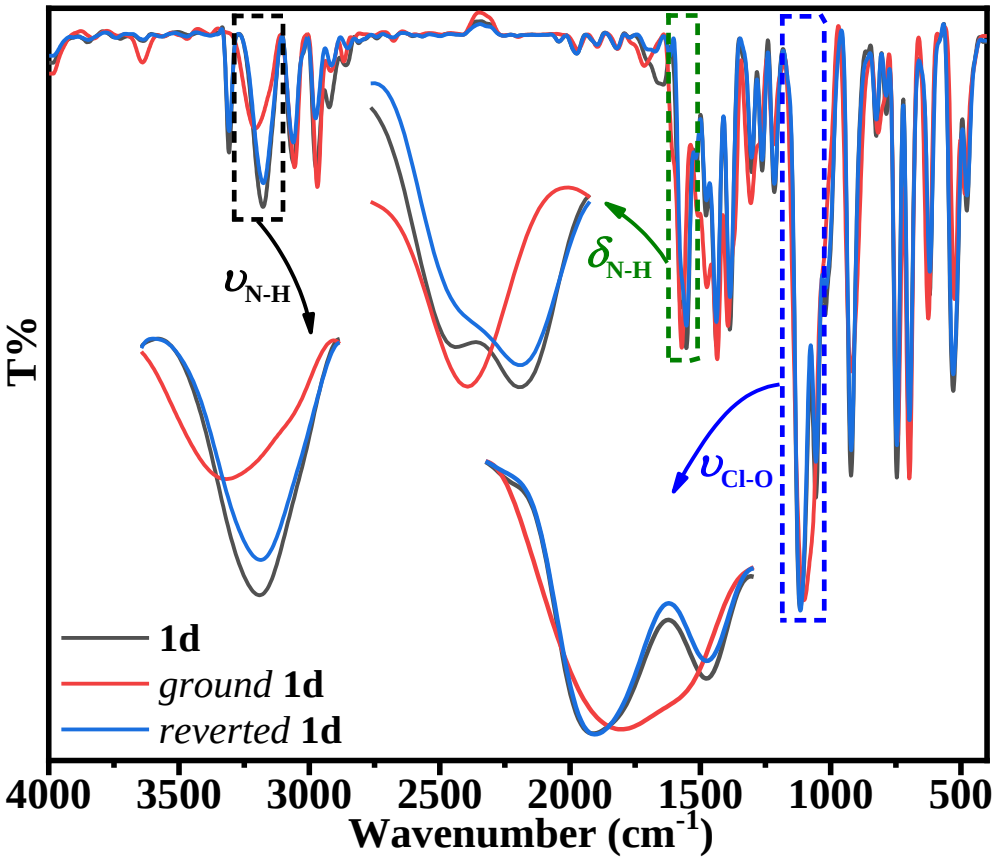

Fig. S12 FT-IR spectra of **1d** in different solid states.

1c	1d
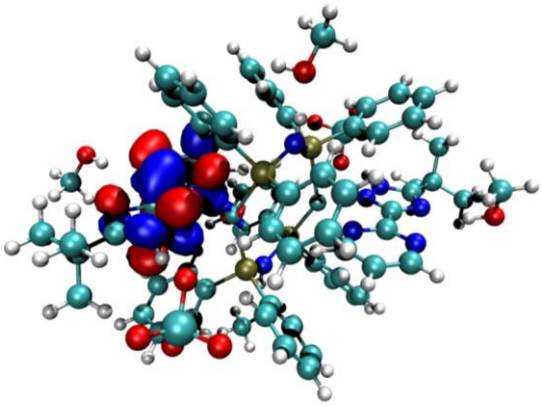	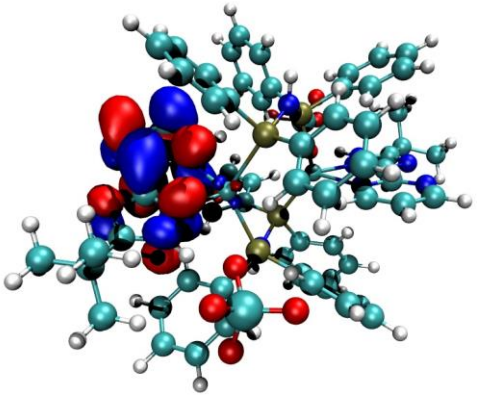
LUMO	LUMO
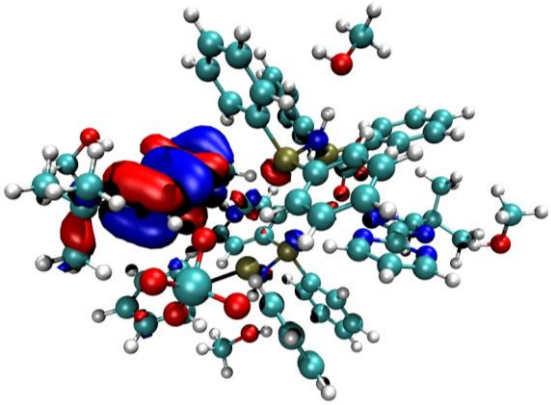	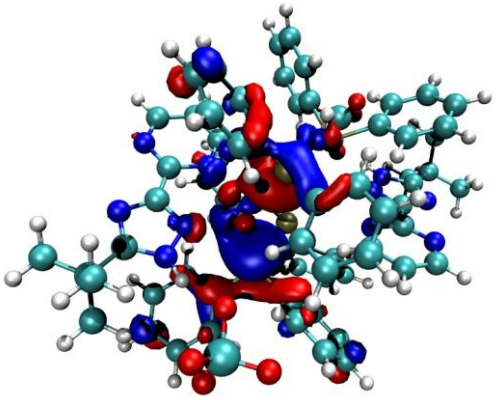
HOMO-2	HOMO
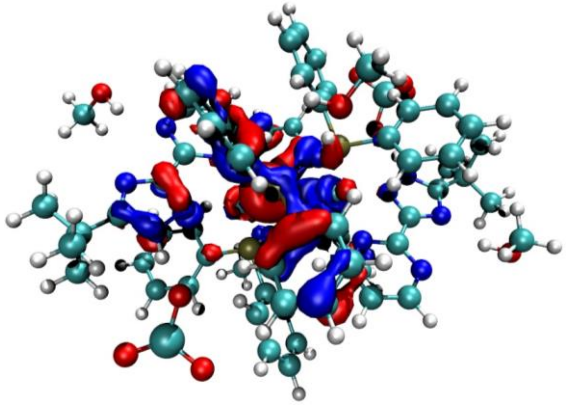	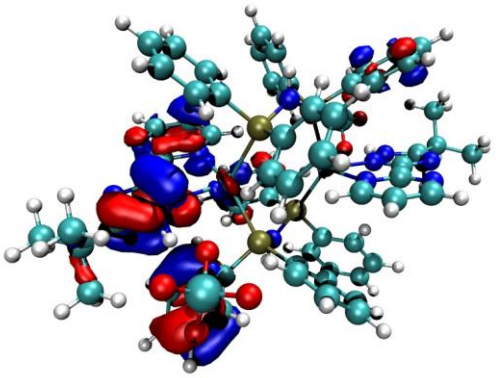
HOMO-3	HOMO-6

Fig. S13 Plots of the frontier molecular orbitals involved in the emissions of **1c** and **1d** by TDDFT method at the M062X level.

Table S1 Crystal data and structure refinement parameters of **1a**–**1d**.

compound	**1a**	**1b**	**1c**	**1d**
formula	$C_{74}H_{84}Cl_2Cu_2N_{12}O_{12}P_4$	$C_{72}H_{84}Cl_2Cu_2N_{12}O_{12}P_4S_2$	$C_{72}H_{84}Cl_2Cu_2N_{12}O_{12}P_4$	$C_{72}H_{76}Cl_{10}Cu_2N_{12}O_8P_4$
fw	1655.39	1695.567	1631.37	1842.994
T (K)	297.46(15)	293.0	293.0	297.0
crystal system	Triclinic	Triclinic	Monoclinic	Triclinic
space group	$P\ \bar{1}$	$P\ \bar{1}$	$P2_1/n$	$P\ \bar{1}$
a (Å)	12.8443(3)	12.8780(8)	13.8862(14)	10.9861(5)
b (Å)	13.3701(3)	13.4796(8)	14.7620(15)	13.9800(6)
c (Å)	13.9219(3)	13.8931(8)	20.0850(2)	16.0424(7)
α (deg)	72.490(2)	72.881(2)	90.000	99.272(4)
β (deg)	67.577(2)	65.962(2)	104.392(3)	105.477(4)
γ (deg)	67.012(2)	67.540(2)	90.000	96.117(4)
V (Å^3)	2001.86(9)	2007.8(2)	3987.9(7)	2314.36(19)
Z	1	1	2	1
ρ_{calc} (g cm^{-3})	1.373	1.402	1.359	1.322
μ (mm^{-1})	0.744	0.793	0.745	0.871
no. reflections collected	58231	30235	60587	26563
no. unique reflections	9157	9183	9222	8082
R_{int}	0.0529	0.0284	0.0474	0.0700
no. observed reflections	9157	9183	9222	8082
no. parameters	588	514	475	548
GOF on F^2	1.056	1.058	1.083	1.059
R_1 [$I > 2\sigma(I)$]	0.0418	0.0422	0.0601	0.0876
wR_2	0.1362	0.1206	0.1928	0.2737

Table S2 Selected bond lengths (Å) and angles (deg) of **1a**–**1d**.

compound	**1a**	**1b**	**1c**	**1d**
Cu1−N1	2.1217(17)	2.1184(19)	2.118(3)	2.127(4)
Cu1−N2	2.2053(17)	2.2140(2)	2.2330(3)	2.229(4)
Cu1−P1	2.2527(5)	2.2539(6)	2.2559(10)	2.2574(13)
Cu1−P2	2.2582(5)	2.2474(6)	2.2588(10)	2.2597(13)
Cu1···Cu1#	3.3176(3)	3.2931(4)	3.2896(7)	3.2818(7)
N1−Cu1−N2	76.61(7)	76.49(7)	76.51(11)	76.73(14)
N1−Cu1−P1	108.43(5)	104.79(6)	107.73(9)	107.70(11)
N1−Cu1−P2	105.16(5)	108.83(6)	106.69(9)	107.58(11)
N2−Cu1−P1	100.28(5)	99.95(6)	98.91(9)	99.98(11)
N2−Cu1−P2	99.95(5)	100.08(6)	100.21(9)	99.11(12)
P1−Cu1−P2	143.91(2)	143.99(2)	143.61(4)	142.82(5)

Table S3 Photoluminescence data of **1a** in different solid states.

state	λ_{em} [nm]	τ [μs]	Φ_{em} [%]	k_r [s^{-1}]	k_{nr} [s^{-1}]
1a	480	10	84	8.4×10^4	1.6×10^4
heated **1a**	459	50	81	1.6×10^4	3.8×10^3
reverted **1a**	483	10	82	8.2×10^4	1.8×10^4
ground **1a**	527	32	2.4	7.5×10^2	3.1×10^4
p-1a	483	10	82	8.2×10^4	1.8×10^4
heated **p-1a**	459	50	80	1.6×10^4	4.0×10^3

Table S4 Partial molecular orbital compositions (%) of the frontier orbitals involved in the emissive states for **1c** calculated by TDDFT method at the M062X level.

Orbital	Bond Type	MO Contribution (%)		
		Cu	dppa	bmptzH
LUMO	π*(bmptzH)	2.45	6.38	90.9
HOMO-2	π(bmptzH)+π(dppa)	5.15	16.6	78.1
HOMO-3	π(dppa)+*d*(Cu)	16.7	68.6	14.0

Table S5 Calculated emission energies and orbital transition analyses of **1c**, **1d**, and *ground* **1d** from TDDFT calculations with M062X functional at the T_1 geometry.

Compound	*E*, nm (eV)	Transition (Contribution)	Assignment	Measured
1c	496 (2.50)	HOMO-2→LUMO (78.0%) HOMO-3→LUMO (11.7%)	^{3}MLCT/^{3}LLCT/^{3}ILCT	494
1d	403 (3.07)	HOMO→LUMO (31.7%) HOMO-6→LUMO (21.3%)	^{3}MLCT/^{3}LLCT/^{3}ILCT	459
ground **1d**	422 (2.93)	HOMO→LUMO (68.9%)	^{3}MLCT/^{3}LLCT	527

Table S6 Partial molecular orbital compositions (%) of the frontier orbitals involved in the emissive states for **1d** calculated by TDDFT method at the M062X level.

Orbital	Bond Type	MO Contribution (%)		
		Cu	dppa	bmptzH
LUMO	π*(bmptzH)	6.36	7.17	86.4
HOMO	π(dppa)+*d*(Cu)	18.6	74.5	6.89
HOMO-6	π(dppa)+π(bmptzH)	6.97	46.3	45.8

Table S7 Partial molecular orbital compositions (%) of the frontier orbitals involved in the emissive states for *ground* **1d** calculated by TDDFT method at the M062X level.

Orbital	Bond Type	MO Contribution (%)		
		Cu	dppa	bmptzH
LUMO	π*(bmptzH)	6.68	8.40	84.8
HOMO	π(dppa)+*d*(Cu)	19.7	71.8	8.41

REFERENCES

(1) S. Kubota, M. Uda, T. Nakagawa, 1,2,4-Triazoles. V. Nuclear magnetic resonance study of N-methyl derivatives of 1,2,4-triazoles, *J. Heterocycl. Chem.*, 1975, **12**, 855–860.

(2) G. Sheldrick, A short history of *SHELX*, *Acta Cryst. Sect. A*, 2008, **A64**, 112–122.

(3) G. Sheldrick, SHELXT: Integrating space group determination and structure solution, *Acta Cryst. Sect. A*, 2014, **70**, C1437.

(4) H. Puschmann, L. J. Bourhis, O. V. Dolomanov, R. J. Gildea, J. A. K. Howard, OLEX2 – a complete package for molecular crystallography, *Acta Cryst. Sect. A*, 2011, **67**, C593.

(5) X. Gu, J. Yao, G. Zhang, Y. Yan, C. Zhang, Q. Peng, Q. Liao, Y. Wu, Z. Xu, Y. Zhao, H. Fu, D. Zhang, Polymorphism-Dependent Emission for Di(p-methoxylphenyl)dibenzofulvene and Analogues: Optical Waveguide/Amplified Spontaneous Emission Behaviors, *Adv. Funct. Mater.*, 2012, **22**, 4862–4872.

(6) Z. Xiong, Y. Li, J. Liang, S. Xiang, Y. Lv, Z. Zhang, Coordination-Guided Conformational Locking of 1D Metal–Organic Frameworks for a Tunable Stimuli-Responsive Luminescence Region, *ACS Appl. Mater. Interfaces*, 2022, **14**, 38098–38104.

(7) Becke, A. D. Density-functional thermochemistry. Ⅲ. The role of exact exchange. *J. Chem. Phys*. **1993**, *98*, 5648–5652.

(8) Runge, E.; Gross, E. K. U. Density-Functional Theory for Time-Dependent Systems. *Phys. Rev. Lett*. **1984**, *52*, 997–1000.

(9) Francl, M. M.; Pietro, W. J.; Hehre, W. J.; Binkley, J. S.; Gordon, M. S.; DeFrees, D. J.; Pople, J. A. Self-consistent molecular orbital methods. XXIII. A polarization-type basis set for second-row elements. *J. Chem. Phys.* **1982**, *77*, 3654–3665.

(10) Hay, P. J.; Wadt, W. R. Ab initio effective core potentials for molecular calculations. Potentials for K to Au including the outermost core orbitals. *J. Chem. Phys*. **1985**, *82*, 299–310.

(11) Casida, M. E.; Jamorski, C.; Casida, K. C.; Salahub, D. R. Molecular Excitation Energies to High-lying Bound States from Time-dependent Density-functional Response Theory: Characterization and Correction of the Time-dependent Local Density Approximation Ionization Threshold. *J. Chem. Phys*. **1998**, *108*, 4439−4449.

(12) Stratmann, R. E.; Scuseria, G. E.; Frisch, M. J. An Efficient Implementation of Time-dependent Density-functional Theory for the Calculation of Excitation Energies of Large Molecules. *J. Chem Phys*. **1998**, *109*, 8218−8224.

(13) Zhao, Y.; Truhlar, D. G. The M06 suite of density functionals for main group thermochemistry, thermochemical kinetics, noncovalent interactions, excited states, and transition elements: two new functionals and systematic testing of four M06-class functionals and 12 other functionals. *Theor. Chem. Acc*. **2008**, *120*, 215−241.

(14) Frisch, M. J.; Trucks, G. W.; Schlegel, H. B.; Scuseria, G. E.; Robb, M. A.; Cheeseman, J. R.; Scalmani, G.; Barone, V.; Petersson, G. A.; Nakatsuji, H.; Li, X.; Caricato, M.; Marenich, A. V.; Bloino, J.; Janesko, B. G.; Gomperts, R.; Mennucci, B.; Hratchian, H. P.; Ortiz, J. V.; Izmaylov, A. F.; Sonnenberg, J. L.; Williams-Young, D.; Ding, F.; Lipparini, F.; Egidi, F.; Goings, J.; Peng, B.; Petrone, A.; Henderson, T.; Ranasinghe, D.; Zakrzewski, V. G.; Gao, J.; Rega, N.; Zheng, G.; Liang, W.; Hada, M.; Ehara, M.; Toyota, K.; Fukuda, R.; Hasegawa, J.; Ishida, M.; Nakajima, T.; Honda, Y.; Kitao, O.; Nakai, H.; Vreven, T.; Throssell, K.; Montgomery, J. A., Jr.; Peralta, J. E.; Ogliaro, F.; Bearpark, M. J.; Heyd, J. J.; Brothers, E. N.; Kudin, K. N.; Staroverov, V. N.; Keith, T. A.; Kobayashi, R.; Normand, J.; Raghavachari, K.; Rendell, A. P.; Burant, J. C.; Iyengar, S. S.; Tomasi, J.; Cossi, M.; Millam, J. M.; Klene, M.; Adamo, C.; Cammi, R.; Ochterski, J. W.; Martin, R. L.; Morokuma, K.; Farkas, O.; Foresman, J. B.; Fox, D. J. *Gaussian 16, Revision A.03*; Gaussian, Inc.: Wallingford, CT, 2016.

(15) Lu, T.; Chen, F. W. Multiwfn: A Multifunctional Wavefunction Analyzer. *J. Comp. Chem*. **2012**, *33*, 580−592.

(16) Humphrey, W.; Dalke, A.; Schulten, K. VMD: Visual molecular dynamics. *J. Mol. Graph*. **1996**, *14*, 33−38.